

# Multi-modal Swarm Coordination via Hopf Bifurcations

Kleio Baxevani and Herbert G. Tanner

Center for Autonomous and Robotics Systems, University of Delaware, USA.

\*Corresponding author(s). E-mail(s): [kleiobax@udel.edu](mailto:kleiobax@udel.edu);  
Contributing authors: [btanner@udel.edu](mailto:btanner@udel.edu);

## Abstract

This paper outlines a methodology for the construction of vector fields that can enable a multi-robot system moving on the plane to generate multiple dynamical behaviors by adjusting a single scalar parameter. This parameter essentially triggers a Hopf bifurcation in an underlying time-varying dynamical system that steers a robotic swarm. This way, the swarm can exhibit a variety of behaviors that arise from the same set of continuous differential equations. Other approaches to bifurcation-based swarm coordination rely on agent interaction which cannot be realized if the swarm members cannot sense or communicate with one another. The contribution of this paper is to offer an alternative method for steering minimally instrumented multi-robot collectives with a control strategy that can realize a multitude of dynamical behaviors without switching their constituent equations. Through this approach, analytical solutions for the bifurcation parameter are provided, even for more complex cases that are described in the literature, along with the process to apply this theory in a multi-agent setup. The theoretical predictions are confirmed via simulation and experimental results with the latter also demonstrating real-world applicability.

**Keywords:** Multi-agent systems, Multi-behavioral systems, Hopf bifurcation

# 1 Introduction

There are instances of multi-robot coordination and control where inter-agent sensing and communication is not feasible. Examples can be found in micro-robotics for the delivery of biochemical payload [1], as well as in social robotics: indeed, the work in this paper is motivated by a specific instance of a child-robot interaction (CRI) problem, where a collection of mobile robots with minimal sensing and communication capabilities is tasked to engage with very young children in play-based activities as shown in Figure 1. A motion of the robot collection that is reactive with respect to that of the child has been shown to attract their interest [2, 3] and in this context, it is important for the robots to often change their behavior in order to maintain engagement with their human subjects. Collective behaviors where robots rotate around the child, move toward them in formation, or scatter along a pattern have been hypothesized to form a library of child-robot interaction (CRI) primitives that can motivate children into physical play-based activity that can serve motor rehabilitation goals [4].

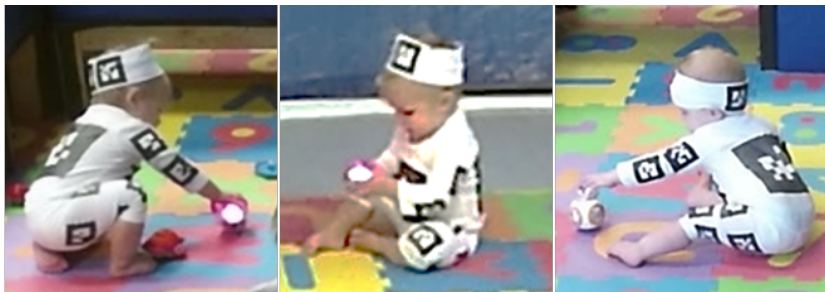


**Fig. 1:** Snapshots of infant interacting with Sphero robot.

Methods for multi-robot control with the objective of converging to a moving geometric formation around a target have been mostly based on local interaction (e.g. [5–7]), often using strategies that impose constant inter-agent bearing [8, 9]—extensions include the utilization of a beacon as a fixed reference [10]—in an effort to control the location of the circumcenter and the radius of the circular orbit. Other pattern-forming approaches have been designed via artificial potential functions and sliding-mode control [11], social interaction [12] or simple self-propelled flocking model of animal collective motion [13]. Elements of bifurcation theory have been also utilized in the literature as a way to form coherent patterns in such multi-agent systems [14–16]. More specifically, there are different collective motions, that can be derived through bifurcation structures for different values of degree of communication. These control schemes, however, depend on agents’ knowledge of other swarm member positions and therefore, are inapplicable when robots cannot communicate or sense each other.

Utilizing commercially available toys as robots in a mini-swarm collective brings challenges due to the robots' limited computation and sensing capabilities, further motivating the use of centralized control architectures similar to those employed in early multi-robot coordination approaches (e.g. [17]). And while generating collective behaviors such as flocking and swarming through decentralized nearest neighbour interactions (for some of the earliest work in this area, see [18–20]) is inherently appealing due to its conceptual links to biological system collectives, in the end, this paradigm may be merely shifting some system vulnerabilities from one place to another: while centralized architectures to cooperative control expose the central coordinator as a single point of failure, the decentralized ones that are based on nearest-neighbour interaction can still in principle be disrupted by blocking the agent interaction mechanisms.

Intuitively, low-level swarm coordination controllers can be realized as artificial velocity vector fields which force the robot to follow a specific behavior by simply following the corresponding flow lines in space [21, 22], i.e., following an Eulerian approach akin to [23]. Such control scheme can be thought of as a universal feedback law broadcast by a central supervisor, that can more easily be tackled with existing design and analysis tools (e.g. [24]), and with a significant benefit of resilience and robustness. At the same time, the inherent robustness of a commercially available toy (robot) in conjunction with the nature of the particular application in which it is utilized may obviate some typical control law requirements such as collision avoidance. In fact, in an application such as this, collisions may actually “add to the fun” of interaction; there have been several other instances where deliberate or unintentional robot collisions have been shown to offer benefits [21, 25, 26].

This paper approaches the problem of coordinating a robot collective over a finite collection of deliberate closed-loop behaviors by designing a reference (velocity) planar vector field to guide the robots, which is capable of realizing the behaviors within the behavior family using the *same* set of differential equations. The latter is motivated by the fact that the formal stability analysis of cooperative control strategies designed to trigger *multiple* collective behaviors in multi-agent systems is challenging due to the switching introduced when transitioning between them, either within some switched system or some hybrid dynamical system modeling formulation [4]. Fundamental properties like existence and uniqueness of solutions, robustness, stability, continuity with respect to initial conditions and parameters, etc., are considerably more difficult to establish in a hybrid framework compared to that of continuous dynamical systems [27]. In cases of multiple robots, the challenge is compounded due to the dimensionality of the system.

Limited existing work along the direction of coordinating a robot using a single evolving time-varying planar vector field [28–30] addresses specific instances of this specific problem by composing point-attractor component vector fields to generate limit cycle behaviors via bifurcation theory, by resetting a

single scalar parameter in the field equations. Cases where the component vector fields can themselves be limit cycles but *do not intersect*, have been studied in our previous work [31, 32]; however, this paper considers the more general case where limit cycles can intersect, it is admittedly significantly more complex [30] and has remained open. The technical contribution of this paper is to show how (planar) limit cycles can be composed using bifurcation theory to produce additional behaviors that are not innate in the component vector fields and demonstrate experimentally that this theory can be utilized to coordinate a collection of mobile robots with very limited sensing and communication capabilities.

The rest of the paper is organized as follows. Section 2 introduces all the preliminary mathematical and dynamical description of the system along with the bifurcation parameters of the system and the mathematical description of the problem considered. The solution approach is subsequently outlined in Section 3, and the main result of the paper appears in Section 4. Numerical and experimental results confirming the theoretical predictions are presented in Section 5. The paper concludes by highlighting a few remarks of this work in Section 6.

## 2 Technical Preliminaries and Problem Formulation

Consider a dynamical system with  $x \in \mathbb{R}^n$  as its state, parameterized by a continuous constant  $\mu \in \mathbb{R}$ :

$$\dot{x} = f_{\mu}(x) . \quad (1)$$

Assume that the system has an equilibrium at  $x_0$  for  $\mu = \mu_0$ .

For the  $x_0$  equilibrium of (1), suppose that the conditions of the following theorem hold (cf. [33, Theorem 3.4.2]):

**Theorem 1** ([33, 34]) *If the Jacobian  $D_x f_{\mu_0} \big|_{x_0}$  of the right-hand-side of (1) has a simple pair of purely imaginary eigenvalues  $\pm i\omega$  for  $\omega > 0$  and no other eigenvalues with zero real parts, then there is a smooth curve of equilibria  $(x(\mu), \mu)$  with  $x(\mu_0) = x_0$ , and the eigenvalues  $\lambda(\mu), \bar{\lambda}(\mu)$  of  $D_x f_{\mu_0}(x(\mu))$  (which are imaginary for  $\mu = \mu_0$ ), vary smoothly with  $\mu$ . If, in addition,*

$$\frac{d}{d\mu} \operatorname{Re} \lambda(\mu) \Big|_{\mu=\mu_0} = d \neq 0 ,$$

*then there exists a unique three-dimensional center manifold passing through  $(x_0, \mu_0) \in \mathbb{R}^n \times \mathbb{R}$ , and a smooth change of coordinates for which the Taylor expansion of (1) of degree 3 on the center manifold, is given in polar coordinates as:*

$$\dot{r} = (d\mu + ar^2)r \qquad \dot{\theta} = \omega + c\mu + br^2 ,$$

*for suitable constants  $a, b$ , and  $c$ . For  $a \neq 0$ , there is a surface of periodic solutions on the center manifold, and*

- *if  $a > 0$ , the periodic solutions are repelling; whereas*
- *if  $a < 0$ , the periodic solutions are stable limit cycles.*

◇

Now, assume that the dynamics of a mobile robot in a hypothesized robot swarm are expressed by equations of the form

$$\dot{\chi} = f(\chi) + G(\chi)u \quad \eta = h(\chi) , \quad (2)$$

where  $\chi \in \mathbb{R}^n$  denotes the robot state,  $\eta \in \mathbb{R}^2$  is a two-dimensional output of interest,  $u \in \mathbb{R}^2$  is the system's two-dimensional control input vector,  $f(\chi) \in \mathbb{R}^n$  is the system's drift vector field, and  $G(\chi) \in \mathbb{R}^{n \times 2}$  is the matrix of control vector fields. We assume that  $f$  and  $G$  are completely known and (2) is not contaminated by noise. For the sake of simplicity, we assume that (2) is input-output feedback linearizable, in which case a state-input transformation can bring the dynamics of the output to the form

$$\dot{\eta} = \nu , \quad (3)$$

where  $\nu \in \mathbb{R}^2$  is the new (transformed) control input. Thus, even if (2) expresses dynamics subject to nonholonomic constraints, by regulating the output of the system, these equations will not affect the control design. At this time, if one prescribes a reference vector field  $F(\eta) \in \mathbb{R}^2$  they can directly force the output of (2) to follow the field lines with a feedback law of the form  $\nu = F(\eta)$  (cf. [35]).

Let  $\eta = (x, y) \in \mathcal{D} \subseteq \mathbb{R}^2$  be a coordinate parameterization of the robot dynamical system's output, and consider *planar vector fields*  $F_i(\eta) : \mathcal{D} \rightarrow T\mathcal{D}$ , for  $i \in \{1, 2\}$ . Each vector field has an *associated (Lyapunov) function*  $f_i : \mathcal{D} \rightarrow \mathbb{R}$  for which it is known that  $\dot{f}_i = \nabla^\top f_i F_i \leq 0$  (equality holds when evaluated at stationary points of  $F_i$ ).

These vector fields are understood as distinct behavior models for the output dynamics (3). In a hybrid system regime, we can imagine switching between  $F_1(\eta)$  and  $F_2(\eta)$ ; here, we will see that we may not only activate either  $F_1$  or  $F_2$  but also *blend* them together in a form of time-varying weighted average, giving rise to unique new behaviors not captured in  $F_1$  or  $F_2$ . In this context, the scalar weights  $m_1$  and  $m_2$  on  $F_1$  and  $F_2$  respectively, are referred to as the *motivation variables*, and each expressing the degree of “commitment” of the system to each of the component vector fields. The motivation variables range in  $[0, 1]$  such that  $m_1 + m_2 + m_U = 1$  with the variable  $m_U$  representing the degree of non-commitment on the part of the system. The *motivation state* of the system is thus defined as the pair  $(m_1, m_2)$ , with the understanding that  $m_i$  can have dynamics of their own and thus evolve over time.

The value dynamics  $v_i$  encodes the “importance” of each model behavior  $F_i$ . It is a positive metric and it grows as the urgency of the task associated with the particular behavior increases. Similarly to the motivation state, the

value state has its own time-varying *value dynamics*:

$$\dot{v}_i = \frac{1}{\lambda_i}(f_i - v_i) , \quad (4)$$

where  $\lambda_i$  is a scale parameter, and  $v_i^* \in \mathbb{R}_+$  is a positive gain.

Based on  $F_i$  and  $m_i$ , the *navigation dynamics* is defined as a new dynamical system formed as a convex combination of  $F_i$  using the motivation state variables  $m_i$  as weights

$$\dot{w} = m_1(t) F_1(w) + m_2(t) F_2(w) . \quad (5)$$

The navigation dynamics (5) codifies the time-varying weighted “blending” of the original model behaviors  $F_1$  and  $F_2$  and expresses the final model reference vector field  $F(\eta)$  for the robots, which will soon be parameterized (and therefore become reconfigurable) through the dynamics of the motivation variables.

Toward this end let  $\sigma \in \mathbb{R}_+$  denote the *bifurcation parameter* and define the *motivation dynamics* as

$$\dot{m}_i = v_i^* v_i m_U - m_i \left[ \frac{1}{v_i^* v_i} - v_i^* v_i m_U + \sigma(1 - m_i - m_U) \right] . \quad (6)$$

With this setup in place, define the set of *mean-difference* coordinates in which the final combined system dynamics will be expressed in:

$$\bar{F} = \frac{F_1(w) + F_2(w)}{2} \quad \Delta F = F_1(w) - F_2(w) \quad (7a)$$

$$\bar{f} = \frac{f_1(w) + f_2(w)}{2} \quad \Delta f = f_1(w) - f_2(w) \quad (7b)$$

$$\bar{m} = \frac{m_1(t) + m_2(t)}{2} \quad \Delta m = m_1(t) - m_2(t) \quad (7c)$$

$$\bar{v} = \frac{v_1(t) + v_2(t)}{2} \quad \Delta v = v_1(t) - v_2(t) , \quad (7d)$$

Now the motivation dynamics-driven reference output system can be expressed in terms of a stack vector  $q = (x, y, \bar{m}, \Delta m, \bar{v}, \Delta v)^\top$ .

Consider a collection of  $N$  robots moving on the plane, each located at  $(x_{r_j}, y_{r_j}, \theta_{r_j})$  for  $j = \{1, \dots, N\}$ , and having unicycle dynamics of the form

$$\dot{x}_{r_j} = v_j \cos \theta_{r_j} \quad \dot{y}_{r_j} = v_j \sin \theta_{r_j} \quad \dot{\theta}_{r_j} = \omega_j . \quad (8)$$

Assume that each robot has an output defined as

$$\eta_j = h_j(x_{r_j}, y_{r_j}) = \begin{bmatrix} x_{r_j} + \varepsilon \cos \theta_{r_j} \\ y_{r_j} + \varepsilon \sin \theta_{r_j} \end{bmatrix} \quad (9)$$

for some small parameter  $\varepsilon > 0$ . It is known that this system is output feedback linearizable and that its internal dynamics are stable as long as  $\eta_j$  remains bounded [36].

The control objective for this robot group is to have each robot follow the flow lines of a reference vector field, appropriately defined through (5). Depending on how it is parameterized, the field should be able to steer them along any one of four different attractors, three of which are distinct planar limit cycles, while the fourth one is a stable node. The designer should be able to select the desired attractor in an online fashion by resetting a finite set of constant field parameters.

### 3 Approach

The solution roadmap adopted for the problem stated above is to use  $F_i$  as two-component vector fields that will model two of the desired planar limit cycles, and blend them in a motivation dynamics approach to produce the whole range of desired spectrum of output reference dynamical behaviors. To this end, we will design navigation, motivation, and value dynamics that together form the desired output reference vector field, which we can regulate by selecting the bifurcation parameter and possibly a set of boundary conditions for the internal dynamics of the output reference vector field.

To construct the right-hand side of (5), first assume for simplicity and without significant loss of generality that two of the three planar limit cycles are circles with identical radius  $r > 0$ . These circles are stable attractors for the vector fields  $F_i$  for  $i = \{1, 2\}$  given as:

$$\begin{aligned}\dot{x} &= r(y - y_{ci}) - (x - x_{ci})[(x - x_{ci})^2 + (y - y_{ci})^2 - r^2] \\ \dot{y} &= -r(x - x_{ci}) - (y - y_{ci})[(x - x_{ci})^2 + (y - y_{ci})^2 - r^2] .\end{aligned}$$

These vector fields can be associated with Lyapunov-like functions of the form

$$f_i(x, y) = \frac{1}{4}[(x - x_{ci})^2 + (y - y_{ci})^2 - r^2]^4 .$$

The next assumption simplifies analysis without loss of generality (it can be enforced via the selection of an appropriate coordinate system):

*Assumption 1*  $(x_{c1}, y_{c1}) = (0, 0)$ ,  $y_{c2} = 0$  and  $x_{c2} = x_{\text{dis}} > 0$ .

The navigation dynamics which serve as a reference vector field for all robots can now be expressed by the following equations in terms of mean-difference coordinates:

$$\begin{aligned}\dot{x} &= \Delta m x_{\text{dis}} \left( \frac{1}{2} r^2 - \frac{3}{2} x^2 + \frac{3}{2} x_{\text{dis}} x - \frac{1}{2} y^2 - \frac{1}{2} x_{\text{dis}}^2 \right) + \bar{m} [r^2 (2x - x_{\text{dis}}) \\ &\quad + 2ry - 2x^3 + 3x^2 x_{\text{dis}} - 2xy^2 - 3x_{\text{dis}}^2 x + y^2 x_{\text{dis}} + x_{\text{dis}}^3] \quad (10a)\end{aligned}$$

$$\begin{aligned}\dot{y} &= \Delta m x_{\text{dis}} \left( -\frac{1}{2} r - xy + \frac{1}{2} y x_{\text{dis}} \right) + \bar{m} (2r^2 y - 2rx + r x_{\text{dis}} - 2x^2 y \\ &\quad + 2xy x_{\text{dis}} - 2y^3 - y x_{\text{dis}}^2) \quad (10b)\end{aligned}$$

8 *Multi-modal Swarm Coordination via Hopf Bifurcations*

$$\begin{aligned} \dot{\bar{m}} = & \frac{1}{4}\sigma(\Delta m^2 - 4\bar{m}^2) + \frac{\Delta m \Delta v(1-2\bar{m})}{4\epsilon_m} - \frac{\epsilon_m(\Delta m + 2\bar{m})}{2(2\bar{v} + \Delta v)} + \frac{\epsilon_m(\Delta m - 2\bar{m})}{2(2\bar{v} - \Delta v)} \\ & + \frac{\bar{v}(1-2\bar{m})(\bar{m}+1)}{\epsilon_m} \end{aligned} \quad (10c)$$

$$\frac{d\Delta m}{dt} = -\frac{\epsilon_m(\Delta m + 2\bar{m})}{2\bar{v} + \Delta v} - \frac{\epsilon_m(\Delta m - 2\bar{m})}{2\bar{v} - \Delta v} - \frac{\bar{v}\Delta m(2\bar{m}-1)}{\epsilon_m} - \frac{\Delta v(2\bar{m}^2 + \bar{m} - 1)}{\epsilon_m} \quad (10d)$$

$$\dot{\bar{v}} = \frac{1}{\epsilon_v}(\bar{f} - \bar{v}) \quad (10e)$$

$$\frac{d\Delta v}{dt} = \frac{1}{\epsilon_v}(\Delta f - \Delta v) \quad (10f)$$

where some symmetry has been forced with the simplifying choice of  $v_1^* = v_2^* = v^*$  and  $\lambda_1 = \lambda_2 = \lambda$ . Setting  $\epsilon_m = 1/v^*$  and  $\epsilon_v = 1/\lambda$ , the dynamics (10) can now be identified as a *singular perturbation* system with  $\epsilon_m, \epsilon_v \in \mathbb{R}_+$  being (assumed independent) infinitesimally small parameters. The two small parameters reveal an interesting two-stage time-scale decomposition.

To identify this and use it to analyze the stability properties of (10) consider first the time-scale decomposition between the subsystem of the pair of what we would call "ultra-fast" variables  $(z_1, z_2) \triangleq (\bar{v}, \Delta v)$  in (10e)–(10f), and that of the "fast" variable  $w_1 \triangleq \bar{m}$  in (10c). In the limit as  $\epsilon_v \rightarrow 0$ , notice that  $(z_1, z_2) \rightarrow (\bar{f}, \Delta f)$  exponentially, and the dynamics of the fast (but still slower than  $z_i$ )  $w_1$  reduces to

$$\begin{aligned} \dot{w}_1 = & \frac{1}{4}\sigma(\Delta m^2 - 4w_1^2) + \frac{\Delta m \Delta f(1 - 2w_1)}{4\epsilon_m} - \frac{\epsilon_m(\Delta m + 2w_1)}{4\bar{f}} \\ & + \Delta f + \frac{\epsilon_m(\Delta m - 2w_1)}{2(2\bar{f} - \Delta f)} + \frac{\bar{f}(1 - 2w_1)(w_1 + 1)}{\epsilon_m} \end{aligned} \quad (11)$$

Consider now the subsystem which is also decomposed in terms of time-scales and consists of: the new fast variable  $\tilde{z}_1 \triangleq \frac{1-2w_1}{\epsilon_m}$ , the evolution of which is determined by (11); and the slow variables  $(\tilde{w}_1, \tilde{w}_2, \tilde{w}_3) \triangleq (x, y, \Delta m)$  driven by (10a), (10b), and (10d), respectively. In this subsystem, the fast dynamics can be rewritten as

$$\begin{aligned} \epsilon_m \dot{\tilde{z}}_1 = & -\frac{1}{2}\sigma[\tilde{w}_3^2 - (1 - \epsilon_m \tilde{z}_1)^2] - \frac{1}{2}\tilde{w}_3 \Delta f \tilde{z}_1 + \frac{\epsilon_m(\tilde{w}_3 + 1 - \epsilon_m \tilde{z}_1)}{2\bar{f} + \Delta f} \\ & - \frac{\epsilon_m(\tilde{w}_3 - 1 + \epsilon_m \tilde{z}_1)}{2\bar{f} - \Delta f} - 2\bar{f}\tilde{z}_1 \left( \frac{1 - \epsilon_m \tilde{z}_1}{2} + 1 \right) \end{aligned} \quad (12)$$

In the limit  $\epsilon_m \rightarrow 0$  it can be verified that  $\tilde{z}_1 \rightarrow -\frac{\sigma(\tilde{w}_3^2 - 1)}{\tilde{w}_3 \Delta f + 6\bar{f}}$ , reducing the slow dynamics of this second subsystem to

$$\begin{aligned} \dot{w}_1 = & \tilde{w}_3 x_{\text{dis}} \left( \frac{1}{2}r^2 - \frac{3}{2}\tilde{w}_1^2 + \frac{3}{2}\tilde{w}_1 x_{\text{dis}} - \frac{1}{2}\tilde{w}_2^2 - \frac{1}{2}x_{\text{dis}}^2 \right) + \frac{1}{2} \left[ r^2(2\tilde{w}_1 - x_{\text{dis}}) \right. \\ & \left. + 2r\tilde{w}_2 - 2\tilde{w}_1^3 + 3\tilde{w}_1^2 x_{\text{dis}} - 2\tilde{w}_1 \tilde{w}_2^2 - 3\tilde{w}_1 x_{\text{dis}}^2 + \tilde{w}_2^2 \tilde{w}_1 + x_{\text{dis}}^3 \right] \end{aligned} \quad (13a)$$

$$\begin{aligned} \dot{w}_2 = & -\tilde{w}_3 x_{\text{dis}} \left( \frac{1}{2}r + \tilde{w}_1 \tilde{w}_2 - \frac{1}{2}\tilde{w}_2 x_{\text{dis}} \right) + \frac{1}{2} \left( 2r^2 \tilde{w}_2 - 2r\tilde{w}_1 + r x_{\text{dis}} \right. \\ & \left. - 2\tilde{w}_1^2 \tilde{w}_2 + 2\tilde{w}_1 \tilde{w}_2 x_{\text{dis}} - 2\tilde{w}_2^3 - \tilde{w}_2 x_{\text{dis}}^2 \right) \end{aligned} \quad (13b)$$

$$\dot{\tilde{w}}_3 = -\bar{f}\tilde{w}_3 \frac{\sigma(\tilde{w}_3^2-1)}{\tilde{w}_3\Delta f+3f} - \frac{3}{4}\Delta f \frac{\sigma(\tilde{w}_3^2-1)}{\tilde{w}_3\Delta f+3f} . \quad (13c)$$

Among the equilibria of (13) there are some of particular significance for this analysis:

**Definition 1** An equilibrium  $\tilde{w}_d$  of (13) is called a *deadlock* if  $\tilde{w}_3 = 0$ .  $\diamond$

The following proposition can be shown by direct derivation:

**Proposition 2** One deadlock for (13) is at  $\tilde{w}_d = (x_{\text{dis}}/2, 0, 0)^\top$ .

## 4 Main Results

The Jacobian of the vector field (13) is a 3-dimensional matrix  $J(\tilde{w}) = (J_{ij})$  which is naturally parameterized by  $x_{\text{dis}}$ ,  $r$ , and  $\sigma$ , given (13). Let  $J_d \triangleq J(\tilde{w})|_{\tilde{w}=\tilde{w}_d}$ . For this matrix, we know the following:

**Proposition 3** ([37]) Under the following two conditions on the elements of the system's Jacobian evaluated at the deadlock  $w_d$ ,

$$\begin{aligned} & -J_{11}^2(J_{22} + J_{33}) - J_{22}^2(J_{11} + J_{33}) - J_{33}^2(J_{22} + J_{33}) + J_{11}J_{12}J_{21} + J_{11}J_{13}J_{31} \\ & \quad + J_{22}J_{23}J_{32} + J_{22}J_{12}J_{21} + J_{33}J_{23}J_{32} + J_{33}J_{13}J_{31} \\ & \quad + J_{12}J_{23}J_{31} + J_{21}J_{13}J_{32} - 2J_{11}J_{22}J_{33} = 0 \end{aligned} \quad (14a)$$

$$\text{tr } J_d = J_{11} + J_{22} + J_{33} < 0 , \quad (14b)$$

where  $\text{tr}$  stands for matrix trace,  $J_d$  has two purely imaginary eigenvalues and one real negative eigenvalue.

The left hand side of (14b) reduces to  $\text{tr } J_d = -\frac{3}{16}\sigma + 2r^2 - x_{\text{dis}}^2$ . Condition (14a), on the other hand, is a 2<sup>nd</sup> order polynomial in  $\sigma$  and allows for two possible solutions which can be written with respect to  $x_{\text{dis}}$  and  $r$  in terms of a ratio between two polynomials  $N_1$  and  $N_2$ :

$$\sigma_{1,2} = \frac{N_1(r, x_{\text{dis}})}{2N_2(r, x_{\text{dis}})} , \quad (15)$$

where  $N_2$  is defined as

$$\begin{aligned} N_2(r, x_{\text{dis}}) \triangleq & a_5 r^{18} + a_6 r^{16} x_{\text{dis}}^2 + a_7 r^{14} x_{\text{dis}}^4 + a_8 r^{12} x_{\text{dis}}^6 \\ & + a_9 r^{10} x_{\text{dis}}^8 + a_{10} r^8 x_{\text{dis}}^{10} + a_{11} r^6 x_{\text{dis}}^{12} + a_{12} r^4 x_{\text{dis}}^{14} + a_{13} r^2 x_{\text{dis}}^{16} , \end{aligned}$$

and  $N_1$  is expressed in terms of two other expressions  $P(r, x_{\text{dis}})$  and  $Q(r, x_{\text{dis}})$ , also involving polynomials, as

$$N_1(r, x_{\text{dis}}) \triangleq [P(r, x_{\text{dis}}) \pm Q(r, x_{\text{dis}})] \\ (a_1 r^8 - a_1 r^6 x_{\text{dis}}^2 + a_2 r^4 x_{\text{dis}}^4 + a_3 r^2 x_{\text{dis}}^6 + a_4 x_{\text{dis}}^8)^2 .$$

The auxiliary expressions  $P(r, x_{\text{dis}})$  and  $Q(r, x_{\text{dis}})$  as follows. First,  $P(r, x_{\text{dis}})$  is given as

$$P(r, x_{\text{dis}}) \triangleq \frac{H_1(r, x_{\text{dis}})}{H_2(r, x_{\text{dis}})} ,$$

where

$$H_1(r, x_{\text{dis}}) \triangleq p_1 r^{12} + p_2 r^{10} x_{\text{dis}}^2 + r^8 \left( -p_1 x_{\text{dis}}^4 - x_{\text{dis}}^2 \right) + r^6 \left( p_1 x_{\text{dis}}^6 + p_3 x_{\text{dis}}^4 \right) + \\ r^4 \left( p_4 x_{\text{dis}}^8 + p_5 x_{\text{dis}}^6 \right) + r^2 x_{\text{dis}}^8 \left( p_6 x_{\text{dis}}^2 + p_7 \right) + p_8 x_{\text{dis}}^{12} ,$$

and

$$H_2(r, x_{\text{dis}}) \triangleq r^8 - r^6 x_{\text{dis}}^2 + p_9 r^4 x_{\text{dis}}^4 + p_{10} r^2 x_{\text{dis}}^6 + p_{11} x_{\text{dis}}^8 .$$

Then  $Q(r, x_{\text{dis}})$  is defined as

$$Q(r, x_{\text{dis}}) \triangleq \sqrt{\frac{H_3(r, x_{\text{dis}})}{H_4(r, x_{\text{dis}})}} ,$$

in which

$$H_4(r, x_{\text{dis}}) \triangleq (r^8 - r^6 x_{\text{dis}}^2 + p_9 r^4 x_{\text{dis}}^4 + p_{10} r^2 x_{\text{dis}}^6 + p_{11} x_{\text{dis}}^8)^2 ,$$

and

$$H_3(r, x_{\text{dis}}) \triangleq q_1 r^{22} + r^{20} (x_{\text{dis}}^4 + q_3 x_{\text{dis}}^2) + r^{18} (q_4 x_{\text{dis}}^4 + q_5 x_{\text{dis}}^6) + r^{16} (q_6 x_{\text{dis}}^8 \\ + q_7 x_{\text{dis}}^6 + x_{\text{dis}}^4) + r^{14} (q_8 x_{\text{dis}}^4 + q_9 x_{\text{dis}}^2 + q_{10}) x_{\text{dis}}^6 + r^{12} (q_{11} x_{\text{dis}}^4 \\ + q_{12} x_{\text{dis}}^2 + q_{13}) x_{\text{dis}}^8 + r^{10} (q_{14} x_{\text{dis}}^4 + q_{15} x_{\text{dis}}^2 + q_{16}) x_{\text{dis}}^{10} \\ + r^8 (q_{17} x_{\text{dis}}^4 + q_{18} x_{\text{dis}}^2 + q_{19}) x_{\text{dis}}^{12} + r^6 (q_{20} x_{\text{dis}}^4 + q_{21} x_{\text{dis}}^2 + q_{22}) x_{\text{dis}}^{14} \\ + r^4 (q_{23} x_{\text{dis}}^4 + q_{24} x_{\text{dis}}^2 + q_{25}) x_{\text{dis}}^{16} + r^2 (q_{26} x_{\text{dis}}^2 + q_{27}) x_{\text{dis}}^{20} .$$

The values for the coefficients in those expressions are given in Table 1.

To trigger the different dynamical behaviors of interest in (13), we need these dynamics to be able to undergo a (Hopf) bifurcation through the choice of  $\sigma$ . Whether a critical  $\sigma$  exists to initiate such a bifurcation depends on the choice of  $x_{\text{dis}}$  and  $r$ . When  $Q(r, x_{\text{dis}}) < 0$ , the solutions (15) are complex and are therefore discarded—in this case no Hopf bifurcation can be triggered for the particular choice of  $(x_{\text{dis}}, r)$ . According to (14b), for a Hopf bifurcation to exist, even when both solutions (15) are real, the values of the system and bifurcation parameters should satisfy

$$\sigma < \frac{S_1(r, x_{\text{dis}})}{S_2(r, x_{\text{dis}})} , \quad (16)$$

$i$	$a_i$	$p_i$	$q_i$	$q_{14+i}$
1	0.75	$0.\bar{6}$	$-0.\bar{4}$	-0.50434
2	0.28125	$-0.\bar{3}$	$0.69\bar{4}$	-0.3125
3	-0.046875	0.75	$-1.\bar{3}$	0.187039
4	0.00292969	-0.236979	3.2	0.134657
5	0.03125	-0.1875	-2.5	0.0585938
6	0.015625	0.0377604	3.88194	-0.0322401
7	-0.101563	0.015625	$-1.69\bar{4}$	-0.0207587
8	0.109375	-0.00227865	-3.44097	-0.00585938
9	-0.0598145	0.375	-0.559028	0.00359133
10	0.0196533	-0.0625	-1.5	0.00174967
11	-0.00405884	0.00390625	1.93989	0.000244141
12	0.000518799		1.00868	-0.000233968
13	-0.0000376701		0.9375	-0.0000627306
14			-0.730686	

**Table 1:** The values of the coefficients in polynomials  $N_1$ ,  $N_2$ ,  $H_1$ ,  $H_2$ ,  $H_3$ , and  $H_4$ .

where

$$S_1(r, x_{\text{dis}}) = s_1 r^{10} + s_2 r^8 x_{\text{dis}}^2 + s_3 r^6 x_{\text{dis}}^4 + s_4 r^4 x_{\text{dis}}^6 + s_5 r^2 x_{\text{dis}}^8 + s_6 x_{\text{dis}}^{10}$$

$$S_2(r, x_{\text{dis}}) = s_7 r^8 - s_7 r^6 x_{\text{dis}}^2 + s_8 r^4 x_{\text{dis}}^4 + s_9 r^2 x_{\text{dis}}^6 + s_{10} x_{\text{dis}}^8,$$

with coefficients given in Table 2.

	$i$				
	1	2	3	4	5
$s_i$	1.5	-2.25	1.3125	-0.375	0.0527344
$s_{5+i}$	-0.00292969	0.125	0.046875	-0.0078125	0.000488281

**Table 2:** The coefficients of polynomials  $S_1$  and  $S_2$  that appear in (16).

Ultimately, a real solution of (15) which satisfies (16) signifies the existence of a Hopf bifurcation and becomes the critical value for the bifurcation parameter  $\sigma$ .

## 5 Validation

This section aims at demonstrating numerically and experimentally that appropriate changes in  $\sigma$  give rise to different desired reference vector fields for the robot outputs. Subsequently, straightforward vector field tracking controllers can be used to make a multi-robot system exhibit multiple different behaviors at will, without fundamentally changing its underlying continuous dynamics.

## 5.1 Simulation Results

Consider two vector fields admitting circular limit cycles, and parameterized with  $x_{\text{dis}} = 2.5$  and  $r = 1.4$ . Based on Proposition 2 there should be a deadlock located at  $\tilde{w}_d = (1.25, 0)^T$ ; after substituting the parameters  $(x_{\text{dis}}, r) = (2.5, 1.4)$ , in the analytical form for  $\sigma$ , the critical bifurcation parameter is found to be  $\sigma_c = 0.0434$ , satisfying both conditions of [33, Theorem 3.4.2] since the eigenvalues of the Jacobian turn out as:

$$\lambda_{1,2} = \pm 0.788 i, \quad \lambda_3 = -2.337, \quad \left. \frac{d\lambda}{d\sigma} \right|_{\sigma=0.0434} = -7.9 \neq 0.$$

When  $\sigma < \sigma_c$ , the trajectories of the navigation dynamics (13) converge to a point attractor. When  $\sigma > \sigma_c$ , the trajectories of (13) converge to a (new) limit cycle –distinct from  $F_1$  and  $F_2$ .

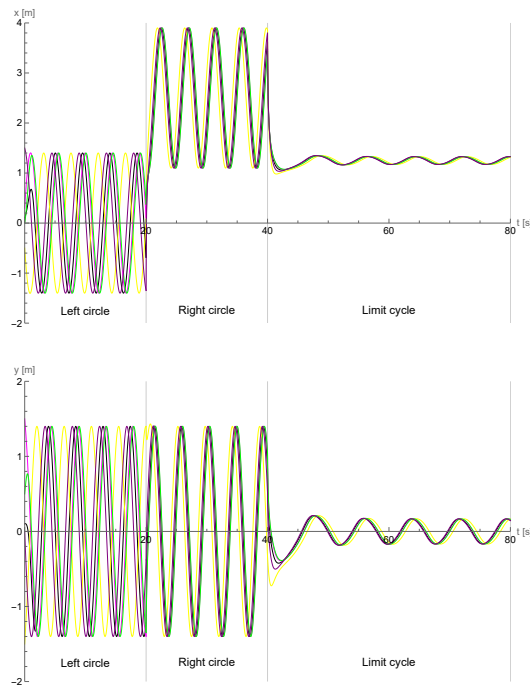


**Fig. 2:** (Simulation results) Evolution of navigation dynamics over time. From  $t_0 = 0$  s to  $t_1 = 20$  s the robot is following the circular field centered at the origin. At  $t_1 = 20$  s its behavior changes and the robot is moving on the second circular field centered at  $(2.5, 0)$  until  $t_2 = 40$  s when it switches to following a limit cycle around the deadlock  $(1.25, 0)$ .

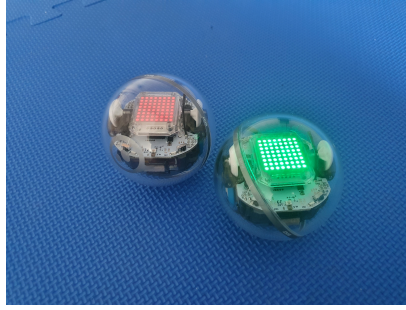


**Fig. 3:** Sphero Bolt: A commercially available educational robotic toy.

The scenario explored in this section is the following: five robots with dynamics (8) and output (9) initially start at  $t = 0$  from different initial positions on the  $x$ - $y$  plane. After input-output feedback linearization, the control is chosen as  $\nu_j = \frac{dw}{dt}(t, \nu)$ , where the navigation dynamics (5) is instantiated in different ways over time to give rise to the desired behavior.

At first the value of  $\Delta m$  is kept fixed at 1, so (5) reduces to  $\dot{w} = F_1(w)$ . This choice produces navigation dynamics that steer the group toward the field  $F_1$  with the circular limit cycle centered at the origin. At  $t = 20$  seconds now the value of  $\Delta m$  is reset to -1, (5) now becomes  $\dot{w} = F_2(w)$  and remains so for 20 more seconds. The robot group now follows the  $F_2$  field possessing a circular limit cycle centered at (2.5, 0). Finally, at  $t = 40$ , the dynamics of  $\Delta m$  are let to evolve according to (13c) and the bifurcation parameter is set above the critical value ( $\sigma = 0.05$ ). As a result, the reference vector field which the group is following has now changed to exhibit a limit cycle around the deadlock (1.25, 0). Figure 2 illustrates the evolution of the outputs  $\eta_j$  of the five robots over time.

## 5.2 Experimental Results

The objective of this preliminary experimental trial is to validate the applicability of the vector field approach to multiple physical robots sharing the same workspace and directed by the same navigation dynamics. While the group size in this first trial is minimal ( $n = 3$ ), it still is indicative of at least two things: (i) physical robots that cannot directly communicate and are unaware of each other's presence can still be coordinated through some shared navigation dynamics, and that (ii) experimental observations match simulation results in terms of the ability of the robots to exhibit different behaviors using the *same* motivation dynamics but with a different value of the bifurcation parameter each time.

The navigation dynamics utilized in this experimental trial are exactly the ones created in simulation, with parameters set as  $x_{\text{dis}} = 2.5$ , and  $r = 1.4$ . Each robot is a Sphero Bolt (Fig. 3), which is essentially a small differential drive robot enclosed in a transparent plastic ball. Such robots are in principle

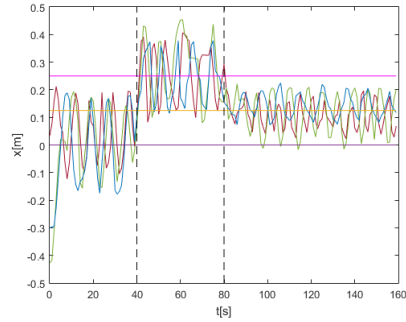
underactuated systems since we only have control over the linear displacement on the longitudinal body axis and yaw. With the right system output, however, (e.g. a point just slightly ahead of the Sphero's center along its  $x$  axis), input-output feedback linearization techniques can be applied to enable full control over this output (see [38]). The robots are equipped with an LED array, which a Zed overhead camera uses to localize them through color detection built-in function of OpenCV library [39], and are directed to track the navigation dynamics reference vector field.

Figure 4 shows the estimated  $x$  and  $y$  planar coordinates of the robots when they follow the field with  $\Delta m = 1$ ,  $\Delta m = -1$  and  $\sigma = 0.05 > \sigma_c$ . The horizontal lines in Fig 4a mark the  $x$ -coordinates  $x = 0$  (where the center of the limit cycle of  $F_1$  lies),  $x = 0.125$  (where the deadlock lies) and  $x = 0.25$  (where the center of the limit cycle of  $F_2$  lies), respectively. Similarly, in Fig 4b the horizontal line at  $y = 0$ , marks the  $y$ -coordinates of the centers of the two limit cycles for  $F_1$ , and  $F_2$ , as well as the  $y$ -coordinate of the deadlock. In both figures, the vertical dashed lines show the times when the behavior of the agents changes due to the reset of the system parameters.

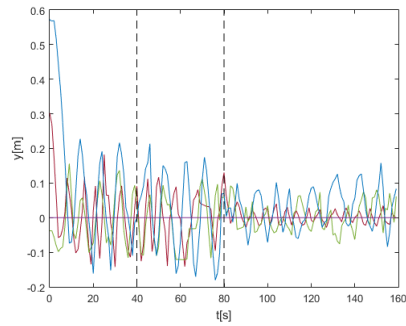
The recorded trajectories are admittedly noisy; this is due not only to the measurement error of the color detection scheme but primarily so because of the inability of these (toy) robots to maintain a precise commanded position. The (bumpy, foamy) nature of the terrain on which the robots are moving also contributes to noise intensity—this type of surface however serves the needs of the pediatric rehabilitation application where these robots are involved in. Collisions do occur in this realization, e.g. when moving along the elliptical limit cycle due to the latter's eccentricity, and such collisions also introduce motion disturbances; currently, it is not our intention to eliminate collisions, but a mathematical roadmap exists for doing so through local field deformations [40].

## 6 Conclusions

Groups of robots that can neither sense nor communicate can still be coordinated to exhibit multiple dynamical behaviors through tunable navigation dynamics, based on velocity fields. This work expands the scope of previous work allowing the composition of circular vector fields that can intersect and provides closed-form analytical expressions for the critical value of bifurcation parameter, informing the designer on how exactly to reset a single value in the equations of motion in order to trigger the switch in the dynamical behavior and coordinate groups of minimally instrumented robots through a common feedback control law that does not rely on robot-to-robot interaction. Additionally, this methodology, provides a more efficient way to better engineer the structure and location of the resulting equilibria, since given the location of the bifurcation deadlock, they can reconfigure the location of the component vector fields blended through the motivation dynamics approach and compute its bifurcation parameters. Such capability can be critical for transferring the theory into the applications of real systems and mobile robot control.



(a)



(b)

**Fig. 4:** (Experimental results) Evolution of three Sphero robots steered by the navigation dynamics. For the first 40 seconds the robots follow the first circular field  $F_1$ , at  $t_1 = 40$  s (first dashed line) their behavior changes to follow the second circular field  $F_2$  for another 40 seconds and finally at  $t_2 = 80$  s (second dashed line) their behavior changes to follow a limit cycle for the last 80 s of the experiment.

## Acknowledgments

This work is supported by the National Science foundation's Smart and Connected Health program via award # 2014264.

## References

- [1] Das, S., Hunter, E.E., DeLateur, N.A., Steager, E.B., Weiss, R., Kumar, V.: Cellular expression through morphogen delivery by light activated magnetic microrobots. *Journal of Micro-Bio Robotics* **15**(2), 79–90 (2019)
- [2] Kokkoni, E., Mavroudi, E., Zehfroosh, A., Galloway, J.C., Vidal, R., Heinz, J., Tanner, H.G.: GEARing smart environments for pediatric

- motor rehabilitation. *Journal of Neuroengineering and Rehabilitation* **17**(1), 16 (2020)
- [3] Kokkoni, E., Zehfroosh, A., Kannappan, P., Mavroudi, E., Galloway, J.C., Heinz, J., Vidaly, R., Tanner, H.G.: Principles for building “smart” learning environments in pediatric early rehabilitation. *Robotics: Science and Systems; Workshop on Perception and Interaction Dynamics in Child-Robot Interaction* (2017)
- [4] Zehfroosh, A., Tanner, H.G.: Reactive Motion Planning for Temporal Logic Tasks Without Workspace Discretization. In: *Proceedings of the IEEE American Control Conference*, pp. 4872–4877 (2019)
- [5] Tanner, H., Christodoulakis, D.: Cooperation Between Aerial and Ground Vehicle Groups for Reconnaissance Missions. In: *Proceedings of the IEEE Conference on Decision and Control*, pp. 5918–5923 (2006)
- [6] Valbuena Reyes, L.A., Tanner, H.G.: Flocking, formation control, and path following for a group of mobile robots. *IEEE Transactions on Control Systems Technology* **23**(4), 1268–1282 (2015)
- [7] Yadav, I., Tanner, H.G.: Mobile Radiation Source Interception by Aerial Robot Swarms. In: *Proceedings of the 2nd IEEE International Symposium on Multi-Robot and Multi-Agent Systems*, pp. 63–69 (2019)
- [8] Marshall, J.A., Broucke, M.E., Francis, B.A.: Formations of vehicles in cyclic pursuit. *IEEE Transactions on Automatic Control* **49**(11), 1963–1974 (2004)
- [9] Halder, U., Schlotfeldt, B., Krishnaprasad, P.: Steering for beacon pursuit under limited sensing. In: *Proceedings of the IEEE 55th Conference on Decision and Control*, pp. 3848–3855 (2016)
- [10] Galloway, K.S., Dey, B.: Collective motion under beacon-referenced cyclic pursuit. *Automatica* **91**, 17–26 (2018)
- [11] Gazi, V.: Swarm aggregations using artificial potentials and sliding-mode control. *IEEE Transactions on Robotics* **21**(6), 1208–1214 (2005)
- [12] Topaz, C.M., Bertozzi, A.L.: Swarming patterns in a two-dimensional kinematic model for biological groups. *SIAM Journal on Applied Mathematics* **65**(1), 152–174 (2004)
- [13] Virágh, C., Vásárhelyi, G., Tarcai, N., Szörényi, T., Somorjai, G., Nepusz, T., Vicsek, T.: Flocking algorithm for autonomous flying robots. *Bioinspiration & biomimetics* **9**(2), 025012 (2014)

- [14] Edwards, V., deZonia, P., Hsieh, M.A., Hindes, J., Triandaf, I., Schwartz, I.B.: Delay induced swarm pattern bifurcations in mixed reality experiments. *Chaos: An Interdisciplinary Journal of Nonlinear Science* **30**(7), 073126 (2020)
- [15] Szwaykowska, K., Schwartz, I.B., Romero, L.M.-y.-T., Heckman, C.R., Mox, D., Hsieh, M.A.: Collective motion patterns of swarms with delay coupling: Theory and experiment. *Physical Review E* **93**(3), 032307 (2016)
- [16] Schwartz, I.B., Edwards, V., Kamimoto, S., Kasraie, K., Ani Hsieh, M., Triandaf, I., Hindes, J.: Torus bifurcations of large-scale swarms having range dependent communication delay. *Chaos: An Interdisciplinary Journal of Nonlinear Science* **30**(5), 051106 (2020)
- [17] Tanner, H.G., Loizou, S., Kyriakopoulos, K.J.: Nonholonomic navigation and control of cooperating mobile manipulators. *IEEE Transactions on Robotics and Automation* **19**(1), 53–64 (2003)
- [18] Tanner, H.G., Jadbabaie, A., Pappas, G.J.: Stable Flocking of Mobile Agents, Part I: Fixed Topology. In: *Proceedings of the IEEE Conference on Decision and Control*, pp. 2010–2015 (2003)
- [19] Tanner, H.G., Jadbabaie, A., Pappas, G.J.: Stable Flocking of Mobile Agents, Part II: Dynamic Topology. In: *Proceedings of the IEEE Conference on Decision and Control*, pp. 2016–2021 (2003)
- [20] Saber, R.O.: Flocking for multi-agent dynamic systems: algorithms and theory. *IEEE Transactions on Automatic Control* **51**(3), 401–420 (2007)
- [21] Stager, A., Tanner, H.: Composition of Local Potential Functions with Reflection. In: *Proceedings of the IEEE International Conference on Robotics and Automation*, pp. 5558–5564 (2019)
- [22] Panagou, D., Tanner, H.G., Kyriakopoulos, K.J.: Nonholonomic control design via reference vector fields and output regulation. *ASME Journal of Dynamic Systems, Measurement and Control* **137**(8), 2831–2836 (2015)
- [23] Kingston, P., Egerstedt, M.: Index-free multi-agent systems: An eulerian approach. *IFAC Proceedings Volumes* **43**(19), 215–220 (2010)
- [24] Panagou, D., Tanner, H.G., Kyriakopoulos, K.J.: Control of nonholonomic systems using reference vector fields. In: *2011 50th IEEE Conference on Decision and Control and European Control Conference*, pp. 2831–2836 (2011)
- [25] Stager, A., Tanner, H.G.: Stochastic Behavior of Robots that Navigate

- by Interacting with Their Environment. In: Proceedings of the IEEE Conference on Decision and Control, pp. 6871–6876 (2016)
- [26] Karydis, K., Zarouk, D., Poulakakis, I., Fearing, R.S., Tanner, H.G.: Planning with the Star(s). In: Proceedings of the IEEE/RSJ International Conference on Intelligent Robots and Systems, pp. 3033–3038 (2014)
- [27] Goebel, R., Sanfelice, R.G., Teel, A.R.: Hybrid Dynamical Systems. In: Princeton University Press (2012)
- [28] Reverdy, P.B.: A route to limit cycles via unfolding the pitchfork with feedback. In: Proceedings of the American Control Conference, pp. 3057–3062 (2019)
- [29] Reverdy, P.B., Koditschek, D.E.: A dynamical system for prioritizing and coordinating motivations. *SIAM Journal of Applied Dynamical Systems* **17**, 1683–1715 (2018)
- [30] Thompson, C., Reverdy, P.B.: Drive-based motivation for coordination of limit cycle behaviors. In: Proceedings of the IEEE Conference on Decision and Control (CDC), pp. 244–249 (2019)
- [31] Baxevani, K., Tanner, H.G.: Multi-behavioral multi-robot systems driven by motivation dynamics. In: Proceedings of the American Control Conference, (in Print) (2023)
- [32] Baxevani, K., Tanner, H.G.: Bifurcating vector fields driven by time-scale separated motivational dynamics. In: Proceedings of the IFAC World Congress, (in Print) (2023)
- [33] Guckenheimer, J., Holmes, P.: Nonlinear Oscillations, Dynamical Systems, and Bifurcation of Vector Fields. In: Springer-Verlag (1983)
- [34] Verduzco, F.: The First Lyapunov Coefficient for a Class of Systems. In: Triennial IFAC World Congress, pp. 1205–1209 (2005)
- [35] Valbuena, L.R., Tanner, H.G.: Flocking, formation control and path following for a group of mobile robots. *IEEE Transactions on Control Systems Technology* **23**(4), 1268–1282 (2015)
- [36] d’Andréa-Novel, B., Bastin, G., Campion, G.: Modelling and Control of Non Holonomic Wheeled Mobile Robots. In: Proceedings of the 1991 IEEE International Conference on Robotics and Automation, pp. 1130–1135 (1991)
- [37] Baxevani, K., Tanner, H.G.: Constructing continuous multi-behavioral

planar systems through motivation dynamics and bifurcations. In: Proceedings of the IEEE Conference on Decision and Control, pp. 1095–1100 (2021)

- [38] Baxevani, K., Otto, G.E., Tanner, H.G., , Trembanis, A.C.: Development and Field Testing of an Optimal Path Following ASV Controller for Marine Surveys. In: Proceedings of the 2022 IEEE/RSJ International Conference on Intelligent Robots and Systems, pp. 6861–6866 (2022)
- [39] OpenCV Developers Team: Open Source Computer Vision (OpenCV) Library. Available: <http://opencv.org>
- [40] Loizou, S.G.: The navigation transformation. IEEE Transactions on Robotics **33**(6), 1516–1523 (2017)

## Statements and Declarations

### Funding

This work is supported by the National Science foundation’s Smart and Connected Health program via award # 2014264.

### Conflicts of Interest

The authors have no relevant financial or non-financial interests to disclose.

### Code or Data Availability

Not applicable.

### Author’s Contribution

All authors contributed to the study conception and design. Material preparation, data collection and analysis were performed by Kleio Baxevani and Herbert Tanner. The first draft of the manuscript was written by Kleio Baxevani and all authors commented and edited the manuscript. All authors read and approved the final manuscript.

### Ethics approval

This work did not involve human or animal subjects therefore it did not require ethics approval.

### Consent to participate

Not applicable.

### Consent for publication

Not applicable.